Avalanche contribution to shear modulus of granular materials

Michio Otsuki[1,*] and Hisao Hayakawa[2]

[1] *Department of Materials Science, Shimane University, Matsue 690-8504, Japan*
[2] *Yukawa Institute for Theoretical Physics, Kyoto University, Kyoto 606-8502, Japan*

(Dated: February 27, 2014)

Shear modulus of frictionless granular materials near the jamming transition under oscillatory shear is numerically investigated. It is found that the shear modulus G satisfies a scaling law to interpolate between $G \sim (\phi - \phi_J)^{1/2}$ and $G \sim \gamma_0^{-1/2}(\phi - \phi_J)$ for a linear spring model of the elastic interaction between contacting grains, where ϕ, ϕ_J, and γ_0 are, respectively, the volume fraction of grains, the fraction at the jamming point, and the amplitude of the oscillatory shear. The linear relation between the shear modulus and $\phi - \phi_J$ can be understood by slip avalanches.

PACS numbers: 83.80.Fg, 81.40.Jj, 62.29.fq

arXiv:1402.6473v1 [cond-mat.soft] 26 Feb 2014

I. INTRODUCTION

Amorphous materials consisting of densely packed particles such as granular materials [1], colloidal suspensions [2], emulsions, and foams [3] have rigidity above a critical density, while they lose rigidity below the critical density. Such rigidity transition, known as the jamming transition, has attracted much attention among researchers in these days [4].

In the vicinity of the jamming point taking place at the volume fraction of the jamming point ϕ_J, amorphous materials exhibit critical behavior. Assemblies of frictionless particles exhibit a mixed transition, in which the coordination number shows a discontinuous transition, while the pressure, the elastic moduli, and the characteristic frequency of the density of state exhibit continuous transition [5–7]. Moreover, critical scaling laws, similar to those observed in equilibrium critical phenomena, exist in the rheology of the sheared disordered particles [8–22]. On the other hand, assemblies of frictional grains exhibit a discontinuous transition associated with a hysteresis loop and a discontinuous shear-thickening in the rheology under steady shear [23–30].

The shear modulus G, the ratio of the shear stress to the shear strain, is one of the most important quantities to characterize the jamming transition. It is well known that G slightly above the jamming point satisfies the scaling

$$G \sim (\phi - \phi_J)^{1/2} \tag{1}$$

for grains interacted with a linear spring model, where ϕ is the volume fraction [5–7]. This power law as well as the frequency dependence of G can be explained by the analysis of the soft mode, and the validity of these laws are verified through simulations [31, 32]. On the other hand, Refs. [33, 34] have recently reported that G might obey a different power law of the excess volume fraction, $\phi - \phi_J$, as

$$G \sim \phi - \phi_J \tag{2}$$

through an experiment and a simulation of soft spherical particles at finite temperature. The conflict between Eqs. (1) and (2) may be understood from the amplitude of the shear strain. Indeed, conventional studies assume that the contact network is unchanged during the process because of an infinitesimal amplitude of the shear strain, but might be inappropriate for a finite strain even near the jamming point. In fact, as shown in Fig. 1 obtained from a simulation under an oscillatory shear, many bonds between contacting grains near the jamming point are broken under the shear strain γ larger than 10^{-4}, which causes slip avalanches distributed in a broad range of sizes [35–37]. To interpolate previously reported relations, Eqs. (1) and (2), we postulate the scaling for the shear modulus:

$$G(\phi, \gamma_0) = G_0(\phi - \phi_J)^a \mathcal{G}\left(\gamma_0/(\phi - \phi_J)^b\right), \tag{3}$$

where a and b are the critical exponents, γ_0 is the strain amplitude, and G_0 is the characteristic shear modulus, which is determined from the elasticity and the diameter of grains. We also assume that the scaling function $\mathcal{G}(x)$ satisfies

$$\lim_{x\to 0} \mathcal{G}(x) = \text{const.}, \quad \lim_{x\to\infty} \mathcal{G}(x) = x^{-c} \tag{4}$$

with an exponent c. To be consistent with the known results, the exponents may satisfy $a = 1/2$ and $a + bc = 1$, which indicates that G obeys Eq. (2) multiplied by γ_0^{-c} for large strain amplitude. It should be noted that the plastic-elastic rheology of jammed granular materials under large strain amplitude is studied in Ref. [38], but the studies on the dependence of the shear modulus on the shear strain do not exist as long as we know.

In this paper, we numerically study the behavior of the shear modulus G of granular materials near the jamming point ϕ_J under an oscillatory shear. In Sec. II, we explain our setup and model. In Sec. III, we present the details of our numerical results. In Sec. IV, we phenomenologically estimate the values of exponents a, b, and c we

*otsuki@riko.shimane-u.ac.jp

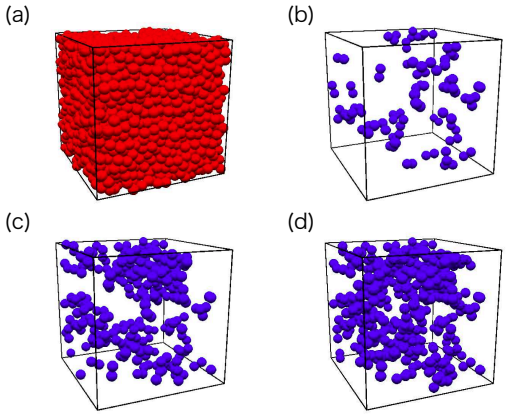

FIG. 1: (Color online) Time evolution of a frictionless granular system of a linear spring between contacting grains for the packing fraction $\phi = 0.660$ under an oscillatory shear, where the jamming fraction ϕ_J is 0.6494. (a) A snapshot of grains without shear strain, i.e. $\gamma = 0$. (b) A snapshot of the grains whose bonds between contacting pairs at $\gamma = 0$ are broken at $\gamma = 1.2 \times 10^{-4}$. (c) A snapshot of the grains whose bonds between contacting pairs at $\gamma = 0$ are broken at $\gamma = 4.8 \times 10^{-4}$. (d) A snapshot of the grains whose bonds between contacting pairs at $\gamma = 0$ are broken at $\gamma = 7.5 \times 10^{-4}$.

have introduced. We determine the values of exponents a and b in Eq. (3) in terms of phenomenological argument in Sec. IV A, and we discuss the exponent c in the asymptotic form (4) caused from the slip avalanches in Sec. IV B. In Sec. V, we discuss and conclude our results. In Appendix A, we explain the method to determine the jamming transition point. In Appendix B, we re-derive the size distribution of the avalanche obtained in Ref. [35].

II. SETUP OF OUR SIMULATION

Let us consider a three-dimensional frictionless granular assembly in a cubic box of the linear size L. The system includes N spherical grains, where each of them has an identical mass m. The position and the velocity of the grain i are, respectively, denoted by $\boldsymbol{r}_i$ and $\boldsymbol{v}_i$. There exist 4 types of grains for diameter, $0.7\sigma_0$, $0.8\sigma_0$, $0.9\sigma_0$, and σ_0, where number of each species is $N/4$. Throughout this paper, we use the volume fraction ϕ to characterize the density of the grains.

Because the grains are frictionless, the contact force has only the normal component of the elastic force $\boldsymbol{f}_{ij}^{(\mathrm{el})}$ and the dissipative force $\boldsymbol{f}_{ij}^{(\mathrm{dis})}$, which are respectively given by

$$\boldsymbol{f}_{ij}^{(\mathrm{el})} = k(\sigma_{ij} - r_{ij})^{\Delta}\Theta(\sigma_{ij} - r_{ij})\boldsymbol{n}_{ij}, \tag{5}$$

$$\boldsymbol{f}_{ij}^{(\mathrm{dis})} = -\eta v_{ij}\Theta(\sigma_{ij} - r_{ij})\boldsymbol{n}_{ij} \tag{6}$$

with the elastic constant k, the viscous constant η, the diameter σ_i of grain i, $\boldsymbol{r}_{ij} \equiv \boldsymbol{r}_i - \boldsymbol{r}_j$, $\boldsymbol{n}_{ij} \equiv \boldsymbol{r}_{ij}/r_{ij}$, $r_{ij} \equiv |\boldsymbol{r}_{ij}|$, $\sigma_{ij} \equiv (\sigma_i + \sigma_j)/2$, and $v_{ij} \equiv (\boldsymbol{v}_i - \boldsymbol{v}_j) \cdot \boldsymbol{n}_{ij}$. Here, $\Theta(x)$ is the Heaviside step function satisfying $\Theta(x) = 1$ for $x \geq 0$ and $\Theta(x) = 0$ for otherwise. The exponent Δ characterizes the elastic repulsive interaction, i.e. $\Delta = 3/2$ for spheres of Hertzian contact force, and $\Delta = 1$ for the linear spring model. Note that the characteristic shear modulus G_0 introduced in Eq. (3) corresponds to $k\sigma_0^{\Delta-2}$.

In this paper, we apply an oscillatory shear along the y direction under the Lees-Edwards boundary condition [39]. As a result, there exists macroscopic displacement only along the x direction. The time evolution of such a system, known as the SLLOD system [39], is given by

$$\frac{d\boldsymbol{r}_i}{dt} = \frac{\boldsymbol{p}_i}{m} + \dot{\gamma}(t) y_i \boldsymbol{e}_x, \tag{7}$$

$$\frac{d\boldsymbol{p}_i}{dt} = \sum_{j \neq i} \{\boldsymbol{f}_{ij}^{(\mathrm{el})} + \boldsymbol{f}_{ij}^{(\mathrm{dis})}\} - \dot{\gamma}(t) p_{i,y} \boldsymbol{e}_x, \tag{8}$$

where $\boldsymbol{p}_i$ and $\boldsymbol{e}_x$ are respectively the peculiar momentum and the unit vector parallel to the x direction.

We use the viscous constant $\eta = 1.0\sqrt{mk\sigma_0^{\Delta-1}}$, which corresponds to the constant restitution coefficient $e = 0.043$ for $\Delta = 1$ in our simulation. We use the leapfrog algorithm, the second-order accuracy in time with the time interval $\Delta t = 0.2\tau$, where τ is the characteristic time of the stiffness, i.e. $\tau = \sqrt{m\sigma_0^{1-\Delta}/k}$. The number N of the particles is 16000 except in Appendix A, where we estimate the jamming point ϕ_J from a finite size scaling. We have verified that the shear modulus is independent of the system size for $N \geq 4000$.

We randomly place the grains in the system as an initial state, and wait until the kinetic energy of each grain becomes smaller than $10^{-14}k\sigma_0^2$. Then, we apply the shear with the shear rate

$$\dot{\gamma}(t) = \gamma_0 \omega \sin(\omega t), \tag{9}$$

where time t is measured from the relaxed static configuration and ω is the angular frequency of the oscillatory shear. From Eq. (9), the shear strain is given by

$$\gamma(t) = \gamma_0 \{1 - \cos(\omega t)\}. \tag{10}$$

We examine the shear modulus for various strain amplitudes $\gamma_0 = 10^0, 10^{-1}, 10^{-2}, 10^{-3}, 10^{-4}$, and 10^{-5} for $\omega\tau = 10^{-4}$ [40]. We analyze the real part of the complex shear modulus [41] (storage modulus) defined by

$$G(\phi, \gamma_0, \omega) = -\frac{\omega}{\pi} \int_{t_0(\gamma_0)}^{2\pi/\omega + t_0(\gamma_0)} dt \frac{S(t)\cos(\omega t)}{\gamma_0}, \tag{11}$$

where $t_0(\gamma_0)$ is the time when $\gamma(t) = 0$ for a strain am-

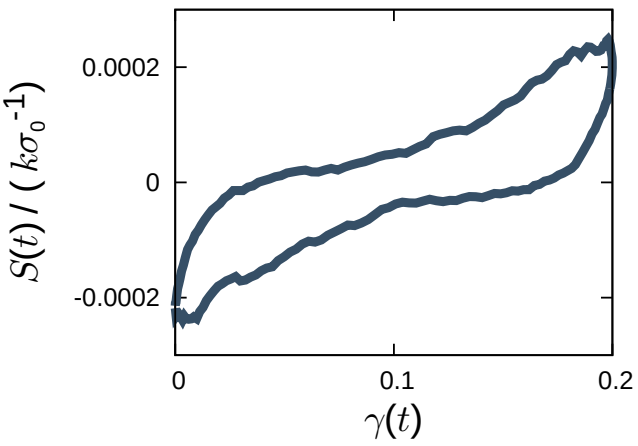

FIG. 2: (Color online) The shear stress $S(t)$ against $\gamma(t)$ with $\phi = 0.652$ and $\gamma_0 = 0.1$ for $\Delta = 1$.

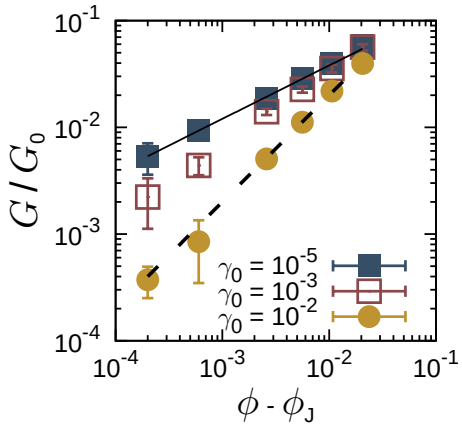

FIG. 3: (Color online) The shear modulus G against the excess volume fraction $\phi - \phi_J$ with $\gamma_0 = 10^{-5}, 10^{-3}$, and 10^{-2} for $\Delta = 1$. The solid and the dashed lines represent the power law functions with the exponent 1/2 and 1, respectively.

plitude γ_0. Here, the shear stress $S(t)$ is calculated from

$$S(t) = -\frac{1}{L^2}\left\langle \sum_i^N \sum_{j>i} r_{ij,x}(t)(f_{ij,y}^{(\mathrm{el})}(t) + f_{ij,y}^{(\mathrm{dis})}(t)) \right\rangle - \frac{1}{L^2}\left\langle \sum_{i=1}^N \frac{p_{x,i}(t)p_{y,i}(t)}{2m} \right\rangle. \quad (12)$$

In this paper, we do not analyze the loss modulus because i) it has only the linear dependence on ω in our simulation and ii) it seems to be independent of density. Note that the stress $S(t)$ exhibits a strong nonlinearity on the strain $\gamma(t)$ as shown in Fig. 2, where we plot the shear stress $S(t)$ against $\gamma(t)$ with $\phi = 0.652$ and $\gamma_0 = 0.1$ for $\Delta = 1$. It should also be noted that G is almost independent of ω for $\gamma_0 \leq 10^{-2}$. We, thus, investigate only γ_0 and ϕ dependence of G in this paper.

III. NUMERICAL RESULTS

In Fig. 3, we plot G against $\phi - \phi_J$ with $\gamma_0 = 10^{-5}, 10^{-3}$ and 10^{-2} for $\Delta = 1$. It should be noted that the jamming point ϕ_J is numerically estimated by the method explained in Appendix A. For the smallest strain amplitude ($\gamma_0 = 10^{-5}$), G reproduces the well known behavior Eq. (1) [6, 31], but G seems to satisfy Eq. (2) for large $\gamma_0 = 10^{-2}$. Thus, it is natural to postulate the scaling form Eq. (2) to interpolate two equations.

Figure 4 shows the scaling plot based on Eq. (3) for $\Delta = 1$. This figure supports the scaling ansatz, Eq. (3), where we have used exponents

$$a = 0.50 \pm 0.02, \quad b = 0.98 \pm 0.02. \quad (13)$$

The exponents are determined by the Levenberg-Marquardt algorithm [42], where we use the functional

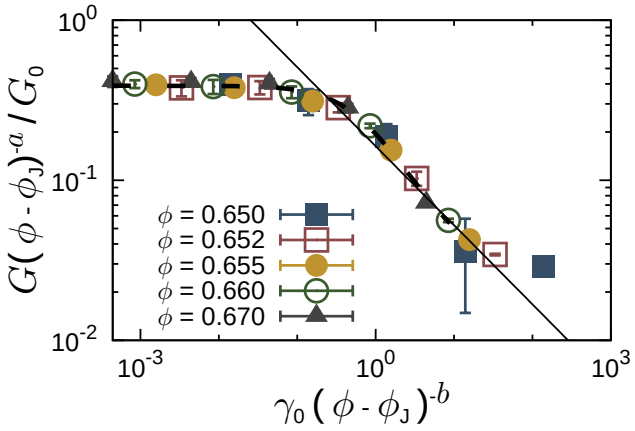

FIG. 4: (Color online) Scaling plot of G characterized by Eq. (3) with $\phi = 0.650, 0.652, 0.655, 0.660$, and 0.670 for $\Delta = 1$. The dashed line is the scaling function given by Eq. (14). The solid line represents the second equation in Eq. (4) with the exponent $c = 0.49$.

form of the scaling function as

$$\mathcal{G}(x) = \frac{B_0}{1 + e^{\sum_{n=1}^3 B_n (\log x)^n}} \quad (14)$$

with fitting parameters $B_0 = 0.39 \pm 0.03$, $B_1 = 1.1 \pm 0.06$, $B_2 = -0.08 \pm 0.04$, and $B_3 = -0.008 \pm 0.008$. From the data of Fig. 4 in the range of $1.0 < \gamma_0/(\phi - \phi_J)^b < 20.0$, we numerically estimate the exponent c in Eq. (4) as

$$c = 0.49 \pm 0.04. \quad (15)$$

In Fig. 4, we plot the solid line with the estimated c. From Eqs. (13) and (15), we obtain $a + bc = 0.98 \pm 0.02$, which also supports Eq. (2).

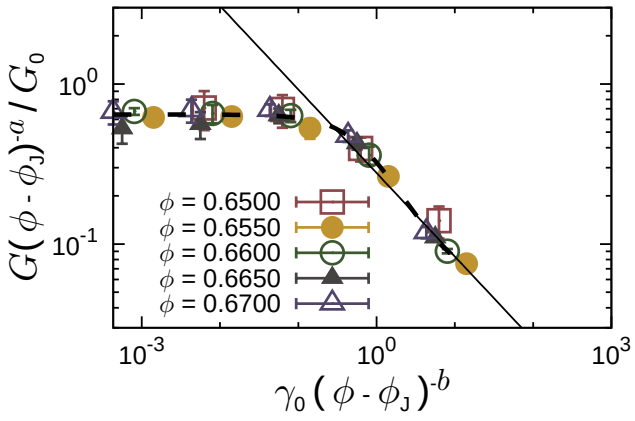

FIG. 5: (Color online) Scaling plot of G characterized by Eq. (3) with $\gamma_0 = 10^{-5}, 10^{-4}, 10^{-3}$, and 10^{-2} for $\Delta = 3/2$. The dashed line is the scaling function given by Eq. (14). The solid line represents the second equation in Eq. (4) with the exponent $c = 0.52$.

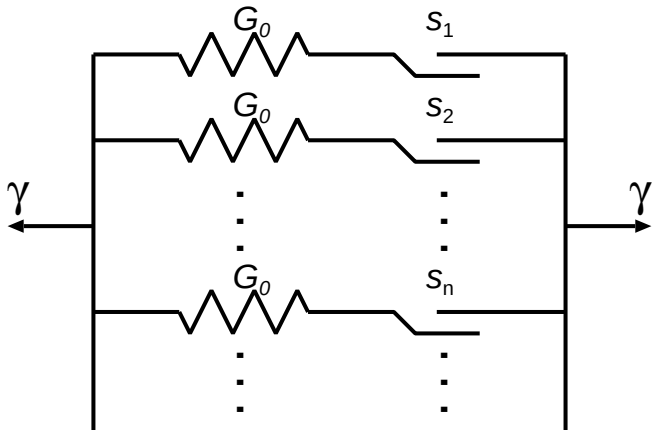

FIG. 6: A schematic picture of a generalized elastic-plastic model consisting of infinite number of series connections with an elastic element of equal shear modulus G_0 and a slip element of unequal yield stress s.

Figure 5 confirms the validity of Eq. (3) for $\Delta = 3/2$, where the scaling exponents are numerically estimated as

$$a = 0.99 \pm 0.02, \quad b = 0.98 \pm 0.01, \quad c = 0.52 \pm 0.03 \quad (16)$$

with the critical fraction $\phi_J = 0.6486 \pm 0.0001$.

IV. PHENOMENOLOGICAL EXPLANATION

In this section, we try to evaluate the exponents for the scaling law Eqs. (3) and (4) in terms of a mean-field like phenomenological argument. In the first part, we derive the exponents a and b in Eq. (3). In the second part, we determine the exponent c in Eq. (4).

A. Exponents a and b

From Eq. (3), G satisfies $G \sim (\phi - \phi_J)^a$ for small strain limit. We also expect $G \sim (\phi - \phi_J)^{\Delta - 1/2}$ in this limit [6]. Thus, we obtain

$$a = \Delta - 1/2. \quad (17)$$

In Eq. (3), we have assumed that the threshold strain $\gamma_c(\phi)$ characterizing the onset of the slip avalanches satisfies $\gamma_c(\phi) \propto (\phi - \phi_J)^b$. We also expect that $\gamma_c(\phi)$ is proportional to the contact length $\ell(\phi)$, which is the average of $\sigma_{ij} - r_{ij}$ between contacting grains. Because $\ell(\phi)$ is expected to satisfy $\sigma(\phi - \phi_J)/(3\phi_J)$ [15], we obtain

$$b = 1. \quad (18)$$

The result of Eqs. (17) and (18) are consistent with the numerical estimation given by Eqs. (13) and (16) for $\Delta = 1$ and $3/2$, respectively.

B. Exponent c

Let us evaluate the exponent c in Eq. (4). For the linear spring model, the exponent should be $c = 1/2$ because of $a + bc = 1$, $a = 1/2$, and $b = 1$ in Eq. (18). However, it seems that Eq. (2) and $a + bc = 1$ cannot be used for the general Δ. Therefore, we should determine the exponent c from an independent argument.

We assume that the shear stress under the oscillatory shear is described by the generalized elastic-plastic model [43] as illustrated in Fig. 6 . Here, the elastic-plastic model consists of infinite number of series connections with an elastic element of equal shear modulus G_0 and a slip element of unequal yield stress s. We assume that the time evolution of the shear stress $S(t)$ is given by

$$S(t) = \int_0^\infty \rho(s) \tilde{S}(s,t)\, ds, \quad (19)$$

where $\tilde{S}(s,t)$ is the stress of an individual element having yield stress s, and $\rho(s)$ is the probability density of the yield stress.

We assume that stress $\tilde{S}(s,t)$ of an individual element for $0 \le t \le 2\pi/\omega$ behaves as a linear function of the strain $\gamma(t)$ given by Eq. (10) until $|\tilde{S}(s,t)|$ reaches the yield stress s. Thus, $\tilde{S}(s,t)$ satisfies

$$\tilde{S}(s,t) = \begin{cases} G_0\ \gamma(t) - s & (0 \le \theta(t) < \theta_c) \\ s & (\theta_c \le \theta(t) < \pi) \\ -G_0\ (\gamma(t) - 2\gamma_0) + s & (\pi \le \theta(t) < \pi + \theta_c) \\ -s & (\pi + \theta_c \le \theta(t) < 2\pi), \end{cases} \quad (20)$$

as illustrated in Fig. 7, where $\theta(t)$ is the phase of the shear strain:

$$\theta(t) = \omega t. \quad (21)$$

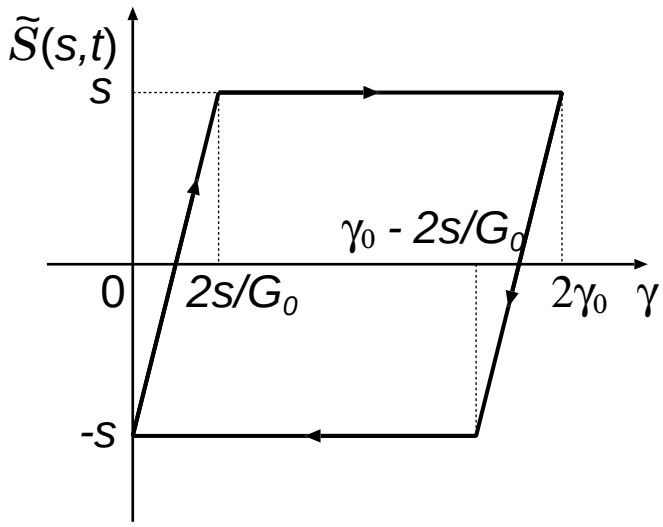

FIG. 7: The stress $\tilde{S}(s,t)$ of an individual element for $0 \leq t \leq 2\pi/\omega$.

The explicit expression of the critical phase θ_c for $S(s,t) = s$ is given by

$$\theta_c\left(s/(G_0\gamma_0)\right) = \cos^{-1}\left(1 - \frac{2s}{G_0\gamma_0}\right), \tag{22}$$

where we have used Eqs. (10), (20), and (21).

The expression of the stress-strain relation (19) depends on the probability density $\rho(s)$. We may assume that $\rho(s)$ behaves qualitatively same as the probability density $\rho_\delta(\delta s)$ of the stress drop δs in slip avalanches [35–37]. (The derivation of $\rho_\delta(\delta s)$ is presented in Appendix B.) Therefore, the yield stress probability density $\rho(s)$ is given by

$$\rho(s) \simeq \begin{cases} A(\phi)s^{-3/2} & (s_{\min}(\phi) \leq s < s_{\max}(\phi)) \\ 0 & (\text{otherwise}), \end{cases} \tag{23}$$

where $A(\phi)$ is the normalization constant satisfying $A(\phi) = 2/[s_{\min}^{-1/2}(\phi) - s_{\max}^{-1/2}(\phi)]$. Note that $A(\phi)$ depends on the volume fraction.

Substituting Eq. (19) into Eq. (11), we obtain

$$G = \int_0^\infty ds \tilde{G}(\gamma_0, s)\rho(s), \tag{24}$$

where $\tilde{G}(\gamma_0, s)$ is the shear modulus of the individual element:

$$\tilde{G}(\gamma_0, s) = -\frac{\omega}{\pi}\int_0^{2\pi/\omega} dt \frac{\tilde{S}(s,t)\cos(\omega t)}{\gamma_0}. \tag{25}$$

Substituting Eq. (20) into Eq. (25), we obtain

$$\tilde{G}(\gamma_0, s) = G_0 F\left(\frac{s}{G_0\gamma_0}\right), \tag{26}$$

where

$$F(x) = \begin{cases} 1 & (x \geq 1) \\ T(x)/\pi & (x < 1) \end{cases} \tag{27}$$

with

$$T(x) = \theta_c(x) - 2\sin\theta_c(x) + \frac{\sin 2\theta_c(x)}{2} + 4x\sin\theta_c(x). \tag{28}$$

Substituting Eqs. (23) and (26) into Eq. (24), we obtain

$$G = A(\phi)G_0\int_{s_{\min}}^{s_{\max}} ds\ s^{-3/2}F\left(\frac{s}{G_0\gamma_0}\right). \tag{29}$$

For $s_{\min}/G_0 \ll \gamma_0 \ll s_{\max}/G_0$, G is approximately given by

$$G \simeq A(\phi)G_0^{1/2}\gamma_0^{-1/2}\int_0^\infty dx\ x^{-3/2}F(x), \tag{30}$$

where we have used the approximate relations $s_{\min}/(G_0\gamma_0) \to 0$ and $s_{\max}/(G_0\gamma_0) \to \infty$. Because the integral in Eq. (30) is apparently converged, we obtain

$$c = 1/2 \tag{31}$$

from Eqs. (3) and (4). This result reproduces the numerical estimation, Eqs. (15) and (16). Thus, Eq. (2) for the general Δ is replaced by

$$G \sim \gamma_0^{-1/2}(\phi - \phi_J)^\Delta. \tag{32}$$

V. DISCUSSION AND CONCLUSION

This section consists of two parts. In the first part, we discuss our results, and we conclude our work in the second part.

A. Discussion

Now, let us discuss our results. First, we discuss the relationship between our result and the scaling law of G proposed in Ref. [32]. Second, we compare our results with those on the power spectrum of the shear stress. Third, we discuss the relationship between our results and the scaling of the yield stress. Finally, we mention the effect of the friction on the scaling for the shear modulus.

Tighe reported that the shear modulus G satisfies a power law of the angular frequency ω for the oscillatory shear at the jamming point:

$$G \sim \omega^{1/2} \tag{33}$$

for an analysis of a model of emulsions [32]. In contrast, both our simulation and phenomenology suggest that the shear modulus is independent of ω. We believe that his

viscous force preventing grains from the rotation and the sliding is the origin of the nontrivial relation (33) [44], which is not involved in our model in Eq. (6). This is the reason for the absence of the ω-dependence of G in our results.

In a simulation and an experiment of granular materials under steady shear [36, 46], the power spectrum of the shear stress exhibits a non-trivial power law dependence on the frequency ω. In contrast, such a dependence of G is not observed in our simulation under oscillatory shear. It should be noted that the power spectrum is directly related to the time correlation of the stress, but the shear modulus G is related with the average of the stress, which is the origin of the different ω-dependences. To study power spectrum of the shear stress would be one of our future subjects.

From Eq. (1) and $\gamma_c(\phi) \sim \phi - \phi_J$, the characteristic stress $S_c(\phi) = G(\phi)\gamma_c(\phi)$ for the appearance of the nonlinear elasticity is expected to be proportional to $(\phi - \phi_J)^{3/2}$ for the linear spring model, which seems to be contradicted with the result of the dynamic yield stress $S_y(\phi) \propto \phi - \phi_J$ under steady shear [14, 15]. However, $S_y(\phi)$ is the shear stress at the steady state with infinitesimal shear rate $\dot{\gamma}$ but finite shear strain because of the relation $\gamma = \lim_{t\to\infty} \dot{\gamma} t$, and is not directly related to $S_c(\phi)$ for small shear strain. This is the reason for the different scalings of $S_c(\phi)$ and $S_y(\phi)$.

It is known that the rheology is drastically affected by friction between particles, at least, for assemblies of soft grains under steady shear [23, 25–29]. The friction plays a key role to cause the shear thickening in rheology, and thus, study on the rheology of frictional grains under an oscillatory shear is practically important. The friction dependence of the scaling law (3) will be discussed elsewhere.

B. Summary

In conclusion, we numerically study the frictionless granular particles and propose a new scaling law which interpolate between $G \sim (\phi - \phi_J)^{\Delta - 1/2}$ for infinitesimal strain and $G \sim \gamma_0^{-1/2}(\phi - \phi_J)^{\Delta}$ for finite strain, where Δ is the exponent to characterize the local elastic interaction between contacting grains. These scaling exponents are verified through our simulation. The scaling of the shear strain under the large strain can be understood by the theory of slip avalanches.

Acknowledgments

The authors thanks B. P. Tighe, K. Kamrin, H. Yoshino, and K. Miyazaki for fruitful discussions. The authors also wish to thank Aspen Center for Physics, where parts of this work is developed. This work was supported by the Grant-in-Aid of MEXT (Grant Nos. 25287098, 22540398, and 25800220) and in part by the Yukawa International Program for Quark-Hadron Sciences (YIPQS). The authors thank the Yukawa Institute for Theoretical Physics at Kyoto University. Discussions during the YITP workshop YITP-W-13-04 on "Physics of glassy and granular materials", YITP-T-13-03 on "Physics of Granular Flows", and YITP-W-10-20 on "Recent Progress in Physics of Dissipative Particles" were useful to complete this work.

Appendix A: Determination of transition point

In this appendix, we explain how to determine the critical volume fraction ϕ_J. Here, we assume that ϕ_J is the volume fraction where the pressure P in the system of $N \to \infty$ becomes finite under sufficiently small and slow shear strain. We, thus, introduce f as the fraction of samples where P is larger than a threshold value $P_{\rm th} = 10^{-6} k\sigma_0^{\Delta-2}$ for $\gamma_0 = 10^{-4}$ and $\omega\tau = 10^{-4}$. Here, P might be approximately given by

$$P = \frac{1}{3L^2}\left\langle \sum_i^N \sum_{j>i} \boldsymbol{r}_{ij} \cdot (\boldsymbol{f}_{ij}^{(\rm el)} + \boldsymbol{f}_{ij}^{(\rm dis)}) \right\rangle + \frac{1}{3L^2}\left\langle \sum_{i=1}^N \frac{|\boldsymbol{p}_i|^2}{2m} \right\rangle. \tag{A1}$$

Figure 8 plots the jammed fraction f against ϕ for $\Delta = 1$, where f is zero for low ϕ and f is finite for large ϕ. It should be noted that the slope of f around $\phi = 0.65$ becomes steeper as the system size increases. In order to determine ϕ_J from the data in Fig. 8, we assume $f(\phi, N)$ satisfies a scaling relation

$$f(\phi, N) = H((\phi - \phi_J)N^{\alpha}) \tag{A2}$$

with an exponent α and a scaling function $H(x)$, which satisfies $\lim_{x\to\infty} H(x) = 1$ and $\lim_{x\to-\infty} H(x) = 0$. Figure 9 verifies the assumption (A2), and thus, we can determine $\phi_J = 0.6494 \pm 0.0001$, where we have assumed the functional form of the scaling function as

$$H(x) = \left\{ 1 + \tanh\left(\sum_{n=0}^{1} A_n x^n \right) \right\}/2 \tag{A3}$$

with the fitting parameters $A_0 = 0.4 \pm 0.2, A_1 = 11 \pm 6$ and $\alpha = 0.66 \pm 0.07$.

Appendix B: Distribution of Avalanche size

In this appendix, we re-derive the probability density $\rho_\delta(\delta s)$ of the stress drop δs obtained in Refs. [35, 36]

1. Setup

In Refs. [35, 36], sheared granular materials are modeled as a simplified lattice system on a coarse-grained

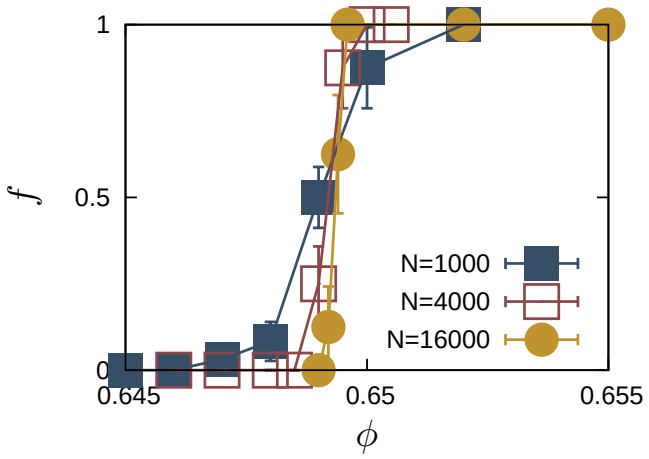

FIG. 8: (Color online) The jammed fraction f against ϕ with different system sizes $N = 1000, 4000$, and 16000 for $\Delta = 1$.

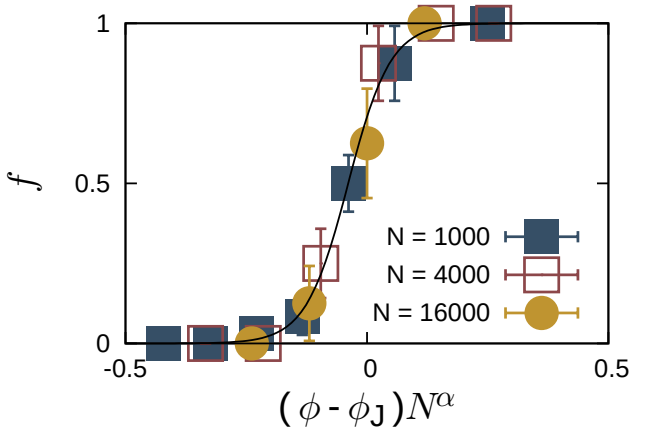

FIG. 9: (Color online) Scaling plot of the jammed fraction f characterized by Eq. (A2) for $\Delta = 1$. The solid line is the scaling function given by Eq. (A3).

scale (larger than the grain diameter) consisting of N' sites and the linear size L. We apply a strain by moving one boundary at a slow speed V (see Fig. 10).

In this setup, the local shear stress s_i at site i under the mean field approximation may be given by

$$s_i = K(Vt - u_i) + \frac{J}{N'}\sum_{j=1}^{N'}(u_j - u_i), \tag{B1}$$

where u_i is the displacement at site i. The first term on the right hand side (RHS) of Eq. (B1) represents the contribution of the global shear under the elastic constant K, which may satisfy the relation $K \sim G_0/L$. The second term on RHS of Eq. (B1) represents the mean-field interaction with the coupling constant J/N'. We can rewrite Eq. (B1) as

$$s_i = KVt + J\bar{u} - (K + J)u_i, \tag{B2}$$

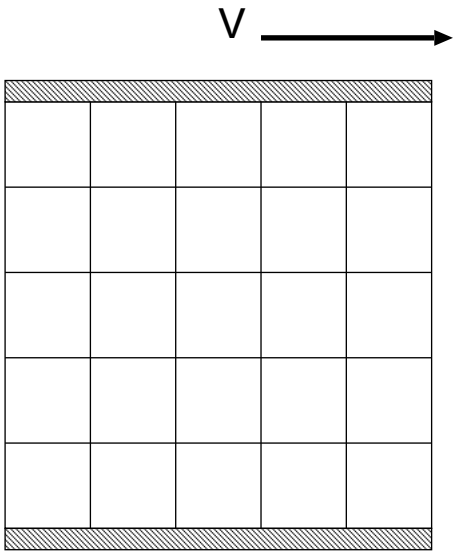

FIG. 10: Illustration of the sheared model lattice.

where we have introduced

$$\bar{u} = \sum_{j=1}^{N'} u_j/N'. \tag{B3}$$

The stress s of the system is defined as the average of s_i:

$$\bar{s} = \frac{1}{N'}\sum_{i=1}^{N'} s_i. \tag{B4}$$

When the local stress s_i is lower than the local yield stress s_y, we regard the site i as a sticked site, where the displacement u_i does not change. As time t increases, the local stress s_i given by Eq. (B2) increases. When the shear stress s_i exceeds s_y, we assume that the site i slips in the shear direction and u_i grows to relax the shear stress s_i to the 'arrest stress' s_a. The time scale for the local slip may be sufficiently small so that Vt in Eq. (B1) is regarded as unchanged during a slip. Thus, the displacement δu_i and the local stress drop $\delta s_{\rm self}$ due to the slip are respectively rewritten as

$$\delta u_i = -\frac{s_y - s_a}{K + J}, \tag{B5}$$

$$\delta s_{\rm self} = -(s_y - s_a), \tag{B6}$$

which leads to the increase of the local stress at the other sites as

$$\delta s_{\rm oth} = C(s_y - s_a)/N' \tag{B7}$$

with

$$C = \frac{J}{J + K}. \tag{B8}$$

Then, the stress drop $\delta s_{\rm slip}$ of the total system is given by

$$\begin{aligned}\delta s_{\rm slip} &= \{-(s_y - s_a) + (N' - 1)\cdot C(s_y - s_a)/N'\}/N' \\ &\simeq -(1 - C)(s_y - s_a)/N'.\end{aligned} \tag{B9}$$

This increase of the local stress may lead to the slip of a site $j \neq i$, and result in a sequential avalanche with n slips, where the stress drop is given by

$$\delta s = (1 - C)(s_{\rm y} - s_{\rm a})n/N'. \tag{B10}$$

2. Derivation of $\rho_\delta(\delta s)$

As time goes on, the system is expected to reach a statistical steady state. In this subsection, we derive the probability of the stress drop δs in the steady state.

Let us consider the distribution of s_i just before the avalanche begins in order to derive the probability of δs. Here, we introduce a variable X_n as

$$X_n = s_{i(n+1)}, \tag{B11}$$

where $i(n)$ is the index of the site that has the nth largest stress (see Fig. 11). The largest value X_0 is $s_{\rm y}$. X_n decreases as n increases with the gap

$$\delta X_n = X_n - X_{n-1}, \tag{B12}$$

which is randomly distributed.

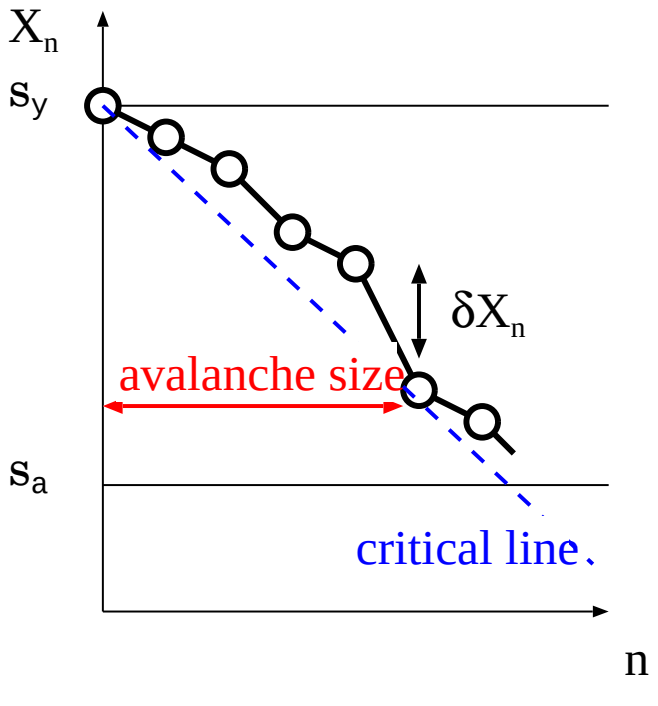

FIG. 11: The schematic illustration of X_n. The solid line is the critical line $s_{\rm y} - n\delta\sigma_{\rm oth}$.

Assuming that s_i is likely to take any allowable value between $s_{\rm a}$ and $s_{\rm y}$, X_n obeys a Poisson process. The probability of the intervals divided by variables obeying a Poisson process satisfies an exponential distribution [45]. Therefore, the distribution of δX_n is given by

$$\rho_X(\delta X_n) = \frac{N'}{s_{\rm y} - s_{\rm a}} e^{-\frac{N'}{s_{\rm y}-s_{\rm a}}\delta X_n}. \tag{B13}$$

When the avalanche starts, the site $i(1)$ slips and the local stress at other sites increases by $\delta s_{\rm oth} = C(s_{\rm y} - s_{\rm a})/N'$. If the local stress at the site $i(2)$ exceeds $s_{\rm y}$ because of the increase of the stress, it slips. This means that the slip proceeds to the site $i(2)$ if X_1 is larger than $s_{\rm y} - \delta s_{\rm oth}$. Similarly, the site $i(n+1)$ slips if X_n is larger than $s_{\rm y} - n\delta s_{\rm oth}$. In Fig. 11, we plot the critical line $s_{\rm y} - n\delta\sigma_{\rm oth}$. Therefore, the size of the avalanche of the sample shown in this figure is given by the length of the region where X_n exceeds the critical line.

In order to obtain the probability distribution of the avalanche size, we define

$$Z_n = X_n - (s_{\rm y} - n\delta s_{\rm oth}). \tag{B14}$$

We plot the schematic illustration of Z_n in Fig. 12. The avalanche size is the length of the region where Z_n exceeds 0. Since Z_n is considered as a biased random walk, the avalanche size is calculated as the first passage time of the biased random walk.

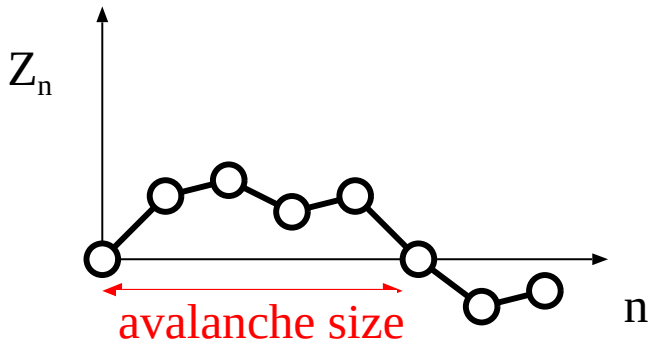

FIG. 12: The schematic illustration of Z_n.

Here, we assume that $\delta Z_n = Z_n - Z_{n-1}$ obeys a Bernoulli trial which has d and $-d$ with the probability p and $1-p$, respectively. Then, the average μ_Z and the variance σ_Z are given by

$$\mu_Z = (2p-1)d, \tag{B15}$$

$$\sigma_Z = d^2. \tag{B16}$$

Because $\delta Z_n = Z_n - Z_{n-1}$ is rewritten with Eq. (B14) as

$$\delta Z_n = -\delta X_n + \delta s_{\rm oth} \tag{B17}$$

and the probability distribution of δX_n satisfies Eq. (B13), μ_Z and σ_Z are respectively given by

$$\mu_Z = -(1-C)\frac{s_{\rm y} - s_{\rm a}}{N'}, \tag{B18}$$

$$\sigma_Z = = \frac{(s_{\rm y} - s_{\rm a})^2}{N'^2}. \tag{B19}$$

From Eqs. (B15), (B16), (B18), and (B19), the probability p and the step size d are respectively given by

$$p = \frac{1}{2}C, \qquad d = \frac{s_{\rm y} - s_{\rm a}}{N'}. \tag{B20}$$

Here, we introduce λ_n as the probability that $Z_n = \sum_{m=1}^{n} \delta Z_n$ becomes negative for the first time at the n-th step. As shown in Ref. [45], such probability for the first passage problem is given by

$$\lambda_{2n} = 0, \tag{B21}$$

$$\lambda_{2n-1} = \frac{1}{2p}\begin{pmatrix} 1/2 \\ n \end{pmatrix}(-1)^{(n+1)}(4pq)^n. \tag{B22}$$

Using Stirling's formula with Eq. (B20), λ_{2n-1} for sufficiently large n is approximately given by

$$\lambda_{2n-1} = \frac{(4pq)^n}{2\pi^{1/2}C}\frac{1}{n^{3/2}}e^{-n/(1-C)^2}. \tag{B23}$$

Because the avalanche size n is proportional to the stress drop δs as shown in (B10), the probability density $\rho_\delta(\delta s)$ of the stress drop δs is thus approximately given by

$$\rho_\delta(\delta s) \simeq \begin{cases} A'\delta s^{-3/2} & (s'_{\rm min} \le \delta s < s'_{\rm max}), \\ 0 & (\text{otherwise}), \end{cases} \tag{B24}$$

where we introduce the cutoff $s'_{\rm max}$ instead of using the exponential term in Eq. (B23) and A' is the normalization constant given as $A' = 2/[(s'_{\rm min})^{-1/2} - (s'_{\rm max})^{-1/2}]$.

[1] H. M. Jaeger, S. R. Nagel, and R. P. Behringer, Rev. Mod. Phys. **68** (1996), 1259.
[2] P. N. Pusey, in *Liquids, Freezing and the Glass Transition, Part II* Les Houches Summer School Proceedings Vol. 51, edited by J. -P. Hansen, D. Levesque, and J. Zinn-Justin (Elsevier, Amsterdam, 1991), Chap. 10.
[3] D. J. Durian and D. A. Weitz, *"Foams," in Kirk-Othmer Encyclopedia of Chemical Technology*, 4th ed., edited by J. I. Kroschwitz (Wiley, New York, 1994), Vol. 11, p. 783.
[4] A. J. Liu and S. R. Nagel, Nature **396** (1998), 21.
[5] C. S. O'Hern, S. A. Langer, A. J. Liu, and S. R. Nagel, Phys. Rev. Lett. **88**, 075507 (2002).
[6] C. S. O'Hern, L. E. Silbert, A. J. Liu, and S. R. Nagel, Phys. Rev. E **68**, 011306 (2003).
[7] M. Wyart, L. E. Silbert, S. R. Nagel, and T. A Witten, Phys. Rev. E **72**, 051306 (2005).
[8] T. S. Majmudar, M. Sperl, S. Luding, and R. P. Behringer, Phys. Rev. Lett. **98**, 058001 (2007).
[9] P. Olsson and S. Teitel, Phys. Rev. Lett. **99**, 178001 (2007).
[10] T. Hatano, M. Otsuki, and S. Sasa, J. Phys. Soc. Jpn. **76**, 023001 (2007).
[11] T. Hatano, J. Phys. Soc. Jpn. **77**, 123002 (2008).
[12] B. P. Tighe, E. Woldhuis, J. J. C. Remmers, W. van Saarloos, and M. van Hecke, Phys. Rev. Lett. **105**, 088303 (2010).
[13] T. Hatano, Prog. Theor. Phys. Suppl. **184**, 143 (2010).
[14] M. Otsuki and H. Hayakawa, Prog. Theor. Phys. **121**, 647 (2009).
[15] M. Otsuki and H. Hayakawa, Phys. Rev. E **80**, 011308 (2009).
[16] M. Otsuki, H. Hayakawa, and S. Luding, Prog. Theor. Phys. Suppl. **184**, 110 (2010).
[17] K. Nordstrom, E. Verneuil, P. Arratia, A. Basu, Z. Zhang, A. Yodh, J. Gollub, and D. Durian, Phys. Rev. Lett. **105**, 175701 (2010).
[18] P. Olsson and S. Teitel, Phys. Rev. E **83**, 030302(R) (2011).
[19] D. Vågberg, P. Olsson, and S. Teitel, Phys. Rev. E **83**, 031307 (2011).
[20] M. Otsuki and H. Hayakawa, Prog. Theor. Phys. Suppl. No. 195, 129 (2012).
[21] A. Ikeda, L. Berthier, and P. Sollich, Phys Rev Lett. **109** 018301 (2012).
[22] P. Olsson and S. Teitel, Phys. Rev. Lett. **109**, 108001 (2012).
[23] M. Otsuki and H. Hayakawa, Phys. Rev. E 83, 051301 (2011).
[24] D. Bi, J. Zhang, B. Chakraborty and R. Behringer, Nature **480**, 355 (2011).
[25] S. Chialvo, J. Sun, and S. Sundaresan, Phys. Rev. E **85**, 021305 (2012).
[26] E. Brown and H. M. Jaeger, Phys. Rev. Lett. **103**, 086001 (2009).
[27] R. Seto, R. Mari, J. F. Morris, and M. M. Denn, Phys. Rev. Lett. **111**, 218301 (2013).
[28] N. Fernandez, R. Mani, D. Rinaldi, D. Kadau, M. Mosquet, H. Lombois-Burger, J. Cayer-Barrioz, H. J. Herrmann, N. D. Spencer, and L. Isa, Phys. Rev. Lett. **111**, 108301 (2013).
[29] C. Heussinger, Phys. Rev. E **88**, 050201 (2013).
[30] M. M. Bandi, M. K. Rivera, F. Krzakala and R.E. Ecke, Phys. Rev. E **87**, 042205 (2013).
[31] M. Wyart, Annales de Physique **30**, 1 (2005).
[32] B. P. Tighe, Phys. Rev. Lett. **107**, 158303 (2011).
[33] T. G. Mason, Matin- D. Lacasse, G. S. Grest, D. Levine, J. Bibette, D. A. Weitz, Phys. Rev. E **56**, 3150 (1997).
[34] S. Okamura and H. Yoshino, arXiv:1306.2777.
[35] K. Dahmen, D. Ertaş, and Y. Ben-Zion, Phys. Rev. E **58**, 1494 (1998).
[36] K. Dahmen, Y. Ben-Zion, and J. T. Uhl, Nat. Phys. **7**, 554 (2011).
[37] A. Dobrinevski, arXiv:1312.7156.
[38] M. Otsuki and H. Hayakawa, AIP Conf. Proc. **1542**, 503 (2013).
[39] D. J. Evans and G. P. Morriss, *Statistical Mechanics of Nonequilibrium Liquids* 2nd ed. (Cambridge University Press, Cambridge, 2008).
[40] In order to obtain the state with γ_0 and ω, we vary the strain amplitude γ_0 from 10^0 to sequentially decreasing values as $\gamma_0 = 10^0, 10^{-1}, 10^{-2}, 10^{-3}, 10^{-4}, 10^{-5}$. For each value of γ_0, we sequentially change the values of the frequency ω as $\omega\tau = 10^{-1}, 10^{-2}, 10^{-3}, 10^{-5}$. At each state with γ_0 and ω, we wait until the waiting time exceeds $8\pi\omega^{-1}$.
[41] M. Doi and S. F. Edwards, *The Theory of Polymer Dy-*

namics (Oxford University Press, Oxford, 1990).
[42] W. H. Press, S. A. Teukolsky, W. T. Vetterling, and B. P. Flannery, *Numerical Recipes*, 3rd ed. (Cambridge University Press, Cambridge, UK, 2007).
[43] V. A. Lubarda, D. Sumarac, and D. Krajcinovic, Eur. J. Mech., A/Solids **12**, 145 (1993).
[44] B. Tighe, arXiv:1205.2960.
[45] W. Feller, *An Introduction to Probability Theory and Its Applications*, 2nd ed. (John Wiley & Sons, Inc., New York, 1957).
[46] F. Dalton and D. Corcoran, Phys. Rev. E **63**, 061312 (2001).